I&EC research
Industrial & Engineering Chemistry Research

Article

Cite This: Ind. Eng. Chem. Res. 2018, 57, 9240−9253

pubs.acs.org/IECR

Monte Carlo Simulations to Examine the Role of Pore Structure on Ambient Air Separation in Metal−Organic Frameworks

Sean M. McIntyre,[†,§] Bohan Shan,[†,§] Ruitong Wang,[‡] Congwei Zhong,[‡] Jichang Liu,*[,‡] and Bin Mu*[,†]

[†]Chemical Engineering, School for Engineering of Matter, Transport, and Energy, Arizona State University, 501 East Tyler Mall, Tempe, Arizona 85287, United States

[‡]State Key Laboratory of Chemical Engineering, East China University of Science and Technology, Shanghai 200237, China

Supporting Information

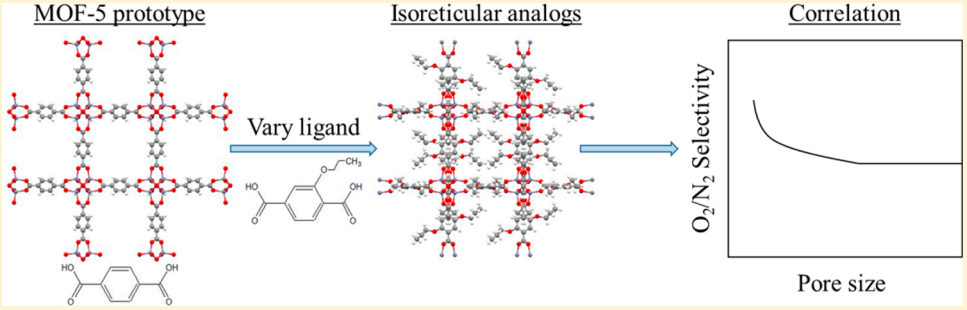

ABSTRACT: MOFs can separate O_2/N_2 mixtures via various mechanisms, making them a great candidate for many air separation applications. We show that the adsorptive behavior of MOFs can be classified based on whether they contain open metal sites (OMSs) and if those sites form a coordination bond with oxygen molecules. Existing data suggests that OMS MOFs that can bind O_2 have high O_2/N_2 selectivity, while OMS MOFs that cannot form such a bond have increased selectivity toward N_2. Monte Carlo simulations show that saturated metal site (SMS) MOFs selectively adsorb O_2 based on dispersion forces. Inaccuracies in simulations on nonbinding OMS MOFs are suggested as evidence that there are other nonbinding interactions impacting O_2/N_2 adsorption in OMS MOFs. Monte Carlo simulations on SMS MOFs are used to define a volume-weighted average pore diameter to establish clear correlations between complex pore size distributions and adsorptive properties.

1. INTRODUCTION

Metal−organic frameworks (MOFs) have been studied extensively for various applications, including separation,[1−7] gas storage,[8,9] catalysis,[10,11] molecular sensing,[12,13] and drug delivery.[14,15] Due to the tunability of the pore structure and chemical properties, as well as high surface area of MOFs, adsorptive separation processes are one of the most exciting potential applications of the materials. However, only a limited number of air separation studies have been performed on MOFs. Here, we show that MOFs exhibit three potential mechanism that can be exploited for equilibrium O_2/N_2 separation: O_2-binding at the metal sites of open metal site (OMS) MOFs, weak O_2-selective van der Waals interactions in saturated metal site (SMS) MOFs, and a third, less-acknowledged, mechanism that results in higher N_2 selectivity in some OMS MOFs.

Air separation has many industrial applications which use purified O_2 and N_2,[16] as well as lower purity applications such as spacecraft cabin oxygen control systems,[17,18] medical oxygen concentrators for life support systems,[19] and tank blanketing in military aircrafts.[16] Oxy-fuel combustion processes utilize purified oxygen rather than air in coal-fired power plants to obtain sequestration-ready CO_2 concentrations in the flue gas and to minimize the formation of NO_x gases.[20] Additionally, purified oxygen is used for steel and paper production, wastewater treatment, and lead and glass production.[16] Purified nitrogen is used in industry for tank blanketing and purging, among other applications.[16] Currently, most high purity O_2 and N_2 are separated via the energy-intensive cryogenic distillation process, although adsorption makes up about 20% of O_2/N_2 production.[16]

O_2-selective carbon molecular sieves (CMSs) are widely used in kinetic adsorption processes for nitrogen generation.[16] The larger diffusivity of O_2 and the difference in equilibrium van der Waals interactions both result in O_2 selectivity in CMS. The larger diffusivity results from the smaller diameter of O_2 allowing it to access adsorption sites more quickly since smaller pores block N_2 from adsorption sites in bigger pores. In principle, a similar mechanism can be exploited in SMS MOFs. We investigate van der Waals interactions in MOFs and offer methods of correlating pore size distributions to equilibrium

Received: March 6, 2018
Revised: June 26, 2018
Accepted: June 26, 2018
Published: June 26, 2018

DOI: 10.1021/acs.iecr.8b00981
Ind. Eng. Chem. Res. 2018, 57, 9240−9253

Table 1. Previously Reported O_2/N_2 Adsorption Data in MOFs[a]

	Framework	O_2		N_2	
		Uptake (mol/kg)	Qst (kJ/mol)	Uptake (mol/kg)	Qst (kJ/mol)
Saturated metal sites	UMCM-1 [21]	0.22	11.0	0.16	5.5
	MOF-177 [22]	0.17	8.0 *	0.15 [23]	7.8 *
	IRMOF-1 *	0.15	8.5	0.13	8.2
	IRMOF-3 *	0.16	9.1	0.14	8.9
	IRMOF-4 *	0.23	14.1	0.17	13.5
	IRMOF-5 *	0.13	12.6	0.11	12.4
	IRMOF-6 *	0.17	9.5	0.15	9.3
	IRMOF-7 *	0.20	10.6	0.16	10.0
	IRMOF-9 *	0.27	11.7	0.22	11.2
	IRMOF-10 *	0.16	7.2	0.14	6.9
	IRMOF-11 *	0.34	14.1	0.23	13.4
	IRMOF-13 *	0.36	13.7	0.31	13.3
	IRMOF-14 *	0.20	8.1	0.18	7.8
	IRMOF-15 *	0.19	7.8	0.17	7.6
	IRMOF-16 *	0.16	6.2	0.14	5.9
	UiO-66 [24]	0.12	8.3 [25]	0.19	-
	HKUST-1(Cu) [26]	0.22	10.7 [27]	0.32	15.0 [27]
	HKUST-1(Fe) [27]	0.35	5.0	0.36	30
	MOF-74(Co) [28]	-	-	-	-
Open metal sites	MIL-100(Fe) [29]	0.25	8.5	0.20	11.5
	MIL-100(Sc) [29]	0.27	15.0	0.21	14.7
	MIL-101(V)† [30]	0.21	-	0.14	-
	Mil-101(V)‡ [30]	0.84	-	-	-
	MOF-74(Fe) [31]	3.26	41.0	0.64	35.0
	HKUST-1(Cr) [32]	3.52	-	0.26	-
	Co(bpbp)-bdc [33]	0.89	88.0	0.02	-
	MIL-101(Cr)@Fc [34]	2.02	-	0.09	-

[a]Uptakes reported at 1 bar, heats of adsorption reported at infinite dilution, highlighted rows are N_2-selective. [b]This study. [c]Activated sample after being exposed to oxygen environment. [d]Activated sample protected in oxygen-free environment.

adsorption properties to compare adsorbents based on this mechanism. 4A zeolite is used in fast PSA processes for nitrogen enrichment (O_2-selective) for tank blanketing, in which a solely kinetic mechanism is used since it is well-established that zeolites are N_2-selective from quadrupole-electric field interactions in equilibrium adsorption processes.[16] This is an important consideration in MOF design for air separation because they can be O_2-selective or N_2-selective based on equilibrium adsorption.

N_2-selective zeolite LiLSX is accepted as the best commercial adsorbent in industrial processes, despite the substantial amount of work needed to separate N_2 from a mixture of ~79% N_2 and ~21% O_2. Adsorption mechanisms that result in O_2 selectivity in MOFs are worth investigating for industrial applications due to the improved efficiency. Johnson Space Center and others have investigated MOFs to reduce the oxygen concentration in air back to ambient levels if therapeutic oxygen supplies must be used within confined spacecrafts.[17,18] O_2-selective MOFs are appropriate for this application because it specifically requires the removal of O_2 from an O_2/N_2 stream. The Air Force currently uses zeolites in their on-board oxygen generating systems.[19] To the knowledge of our research group, there have been no studies focused on the rational design of N_2-selective MOFs for air separation, even though there is evidence for exploitable mechanisms that can achieve this. Some of the previous work on O_2/N_2 adsorption in MOFs is outlined in Table 1.[21−34]

MOFs that contain OMSs after activation interact with O_2 differently than those with coordinatively saturated metal sites. In most cases, OMSs have been shown to have O_2 adsorption properties characteristic of chemisorption (termed "binding" metal sites): strong adsorbent−adsorbate interactions, high initial uptake rate, and large heat of adsorption at low pressure. In chemisorption, the formation of a chemical bond between adsorbate and host material is generally an overwhelmingly stronger interaction than the van der Waals and electrostatic physical interactions. Some MOFs have been shown to have OMSs that are not strong O_2-binding sites (termed "non-binding" metal sites); based on the previous data, it seems that these materials all have increased selectivity toward N_2 over O_2 under ambient conditions.[24,26,27,34] With the definitions of nonbinding vs binding metal site MOFs being used, it can be assumed that both contain OMSs, but only binding metal site MOFs can chemisorb oxygen. SMS MOFs are the counterpart to OMS MOFs in which the metal atoms of a nondefective sample are coordinatively saturated with ligands. SMS MOFs cannot bind with O_2 because the adsorbates cannot access the metal sites. So far, only two MOFs with SMSs have been studied for air separation under the conditions of interest, but each of them selectively adsorbs O_2 over N_2, a property that eluded most zeolites analyzed to date.[16]

The primary motivation of this study was to clarify the dominant interactions that come into play when considering O_2/N_2 equilibrium adsorption in MOFs. We offer insights into the nonbinding interactions between O_2/N_2 and MOFs, so the work is primarily focused on SMS MOFs and nonbinding metal site MOFs. We follow up the work of Sava Gallis et al.,[27] which showed that the OMSs of MOFs are not always strong O_2-binding sites. We begin with a brief literature review to clarify the expected chemisorptive interactions and compare their work to groups who obtained similar results. GCMC adsorption simulations are compared to experiments to show the accuracy for predicting van der Waals interactions in O_2/N_2 adsorption in MOFs. The simulations also show that there is another interaction which was not predicted using generic force field that comes into play for nonbinding metal site

DOI: 10.1021/acs.iecr.8b00981
Ind. Eng. Chem. Res. 2018, 57, 9240−9253

MOFs when the experimentally observed interactions are too weak to be attributed to chemisorption. We compare this finding to similar issues when using GCMC simulations to predict adsorption in OMS MOFs. Finally, we restrict the simulation study to SMS MOFs to analyze the correlation between O_2/N_2 selectivity and pore diameter based on dispersion forces. We define a term called the volume-weighted average accessible (VWAA) pore diameter to clearly show this correlation, and, ultimately, relate the work of Greathouse et al. on adsorption in idealized carbon nanotubes[35] (CNTs) to more complex pore size distributions.

1.1. O_2/N_2 Separation Studies on MOFs with Open Metal Sites. First, we will present a discussion about MOFs with OMSs, in which guest molecules have been removed after activation. This includes MOFs with binding metal sites and MOFs with nonbinding metal sites.

The M_2(dobdc) structure (usually with M = Fe), otherwise denoted as MOF-74, has been shown to selectively coordinate O_2 at the metal sites, but the strong side-on binding results in the irreversible formation of a peroxo species at room temperature.[36−40] $Cr_3(BTC)_2$, commonly referred to as HKUST-1(Cr), is a MOF which chemically binds O_2 with a 30% loss in capacity after 15 temperature swing cycles at room temperature.[31] The use of early transition metals was shown to enhance oxygen binding at the OMSs of mesoporous MIL-100, where the use of Fe ions led to the formation of superoxo-type bonds and Sc led to stronger peroxo bonds.[28] The O_2/N_2 selectivity of MIL-100(Sc) was low compared to other reported chemisorptive MOFs, but the adsorption was fully reversible over 10 cycles.[28] Recent advances in the selection of the electron-donating ligands in Co-MOFs have led to a highly O_2-selective MOF that showed full reversibility in a preliminary cycling experiment up to five temperature swing cycles.[32] Another approach that has been pursued is the encapsulation of O_2-scavenging ferrocene molecules within the large pores of MIL-101 (denoted MOF-101@Fc) to enhance cyclability, but this still led to about a 33% loss in capacity after 15 temperature swing cycles at room temperature.[33] Thus far, no MOFs or related composites have been demonstrated to match the long-term cyclability of previously studied mononuclear cobalt complexes at room temperature.[41]

Even though MOFs with binding metal sites show high oxygen loading capacity, uptake rate, and selectivity, the enhanced interactions often result in cyclability barriers that must be overcome for practical applications. Recent concerns over the inability of life support systems in aircrafts to provide the expected levels of oxygen to pilots are evidence of the need for reliably cyclable sorbents for certain applications.[42] Additionally, the ability of MOFs to bind oxygen in air can make them difficult to implement. The O_2-binding activity of an activated MIL-100(V) sample can decrease substantially when unprotected from an oxygen environment.[43]

The OMSs of MOFs are not always O_2-binding sites. It has been suggested that N_2-selective adsorption in some MOFs under ambient conditions is caused by the presence of OMSs;[21] this is likely similar to the electrostatic interactions that cause nitrogen selectivity of many zeolites in air separation processes.[16] Sava Gallis et al. expected to observe binding of O_2 in the HKUST-1 variants but instead showed weak adsorption energies for O_2 ranging from 10 to 16 kJ/mol and a high value of 30 kJ/mol for N_2 on the Fe-substituted sample.[27] Similarly, the replacement of the Fe ions with Co in the MOF-74 structure led to nonbinding metal sites and a N_2-selective structure.[27] The N_2 selectivity of the highly stable Zr-based MOF, UiO-66,[24] can be explained by the modulated synthesis approach they used resulting in dehydroxylation of the metal clusters and missing-ligand defects.[24] This is an established method of generating OMSs in UiO-66.[44]

We show that there are under-acknowledged physisorptive interactions occurring in OMS MOFs even when they are inactive to oxygen chemisorption, and we relate this interaction to similar results from other groups. Although our results are not enough to give a complete description, the interaction could be an important area of research for future work.

1.2. O_2/N_2 Separation Studies on MOFs with Saturated Metal Sites. Very few SMS MOFs have been analyzed for air separation. $Zn_4O(BTB)_2$, otherwise denoted as MOF-177, was shown to selectively physisorb O_2 over N_2 at room temperature and atmospheric pressure. UMCM-1, another Zn-MOF, contains both BTB and BDC ligands that coordinatively saturate the metal sites; this structure also preferentially physisorbs O_2 over N_2. The reversibility and stability that result from the weak interactions in SMS MOFs motivates a detailed investigation of these novel sorbents for the large number of O_2-selective air separation applications.

The physical adsorption between O_2 and MOFs with SMSs can generally be assumed to be reversible in swing processes at the expense of lower selectivity. The parameters which may affect physisorption of an O_2/N_2 mixture are outlined in Table 2.[45] In the low-pressure regime, dispersion forces are the main

Table 2. Equilibrium Adsorption Properties of O_2 and N_2[33]

	atomic diameter (Å)	dipole moment (D)	quadrupole moment (cm^2)	polarizability ($Å^3$)
O_2	3.01	0	1.3	1.60×10^{-40}
N_2	3.31	0	4.7	1.76×10^{-40}

reason for O_2-selective equilibrium adsorption of the relatively nonpolar gases of interest in SMS MOFs. This is the same behavior as adsorption in nonpolar materials such as CMS and carbon nanotubes. The similarity of the interactions can be rationalized by the fact that adsorbates come in contact with the organic ligands on the surface of SMS MOFs. The work of Greathouse et al.[35] is significant in this discussion because it shows the enhanced adsorption of O_2/N_2 from van der Waals interactions in simple CNT systems with pore sizes near the diameter of these diatomic species. However, the complex pore size distributions of real adsorbent materials and the additional interactions that may come into play in MOFs make it difficult to correlate the impact of pore size on adsorption properties of these materials.

We show that van der Waals interactions are the prominent mechanism for selective adsorption in SMS MOFs and connect the idealized CNT results to more complex pore size distributions by defining the VWAA pore diameter. Specifically, O_2/N_2 selectivity and adsorbent−adsorbate interactions are investigated as a function of VWAA pore diameter to show a clear correlation. We also give recommendations and set goals for the design of MOFs for air separation applications in terms of pore diameter based on these results.

1.3. GCMC Simulations to Predict Adsorption in MOFs. Grand Canonical Monte Carlo (GCMC) simulations can accurately predict equilibrium adsorption in materials by creating an atomic simulation box and holding the chemical potential, volume, and temperature constant, while the number

DOI: 10.1021/acs.iecr.8b00981
Ind. Eng. Chem. Res. 2018, 57, 9240−9253

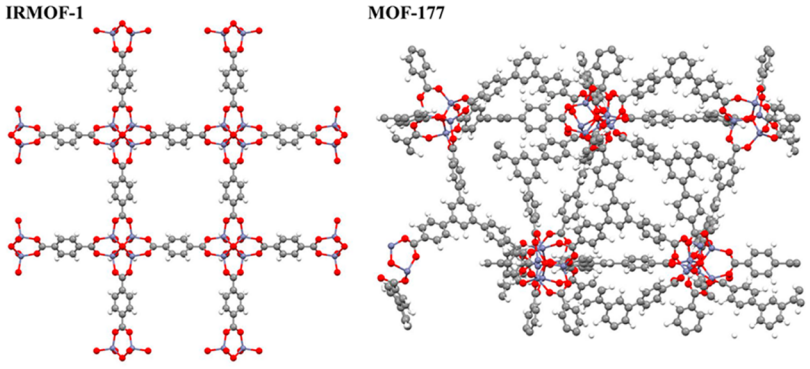

Figure 1. Framework structure of IRMOF-1 (left) and MOF-177 (right) from the *a*-axis.

Table 3. Framework information

Framework	Formula	Ligand	Ligand length (Å)	Catenated?
IRMOF-1	$Zn_4O(BDC)_3$	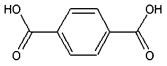	5.75	No
IRMOF-3	$Zn_4O([NH_3]BDC)_3$	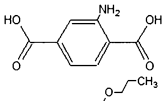	5.691	No
IRMOF-4	$Zn_4O([OC_3H_7]BDC)_3$	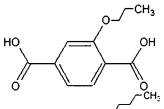	5.784	No
IRMOF-5	$Zn_4O([OC_5H_{11}]BDC)_3$	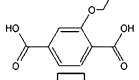	6.512	No
IRMOF-6	$Zn_4O([C_2H_4]BDC)_3$	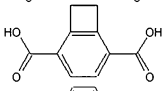	5.789	No
IRMOF-7	$Zn_4O([C_4H_4]BDC)_3$	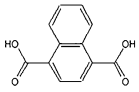	5.53	No
IRMOF-9	$Zn_4O(BPDC)_3$	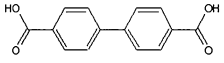	10.047	Yes
IRMOF-10	$Zn_4O(BPDC)_3$	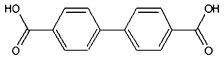	9.9277	No
IRMOF-11	$Zn_4O(HPDC)_3$	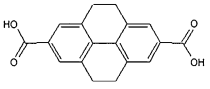	10.044	Yes
IRMOF-12	$Zn_4O(HPDC)_3$	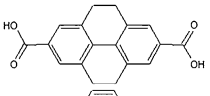	10.049	No
IRMOF-13	$Zn_4O(PDC)_3$		10.032	Yes
IRMOF-14	$Zn_4O(PDC)_3$	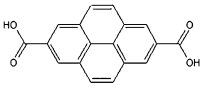	9.881	No
IRMOF-15	$Zn_4O(TPDC)_3$	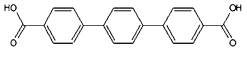	14.3246	Yes
IRMOF-16	$Zn_4O(TPDC)_3$	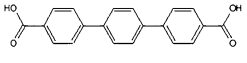	14.222	No

of molecules in the adsorbed phase fluctuates based on a Boltzmann-type probability distribution.[46] Numerous cycles are performed, where each cycle consists of the acceptance or rejection of a translation, rotation, deletion, or insertion move by an adsorbate molecule. The acceptance criterion is a lower energy state in the new configuration. After a number of initialization cycles, the average of the calculated amount of gas adsorbed is computed, representing the equilibrium adsorption capacity under the conditions of interest. The force fields conventionally take into account van der Waals and electro-

DOI: 10.1021/acs.iecr.8b00981
Ind. Eng. Chem. Res. 2018, 57, 9240−9253

static interactions. A variety of electrostatic charge equilibration methods exist that vary substantially in computational complexity; the computation time of these techniques range from seconds to days.[47] Periodic boundary conditions are applied in each direction, which implies the assumption of perfect crystallinity.

Various GCMC simulations have been executed to screen for gas storage and gas separation applications, as well as to offer insights into details of the adsorption mechanism.[48−51] Air separation studies have utilized GCMC simulations in some instances,[27,28,40] yet they are only briefly referenced and included in the Supporting Information; this is likely because many groups are interested in MOFs with OMSs, and the generic force fields used are unable to describe interactions at these sites. The interaction of adsorbates with OMSs has been noted to cause inaccuracies in GCMC simulations.[52,53] The commonly used generic force fields only take into account nonbonding interactions. Also, an in situ neutron diffraction study showed that generic force fields may not properly describe short-range physical interactions at the OMSs.[54] The interactions that have been noted between O_2 and OMSs require reparameterization via a trial-and-error or ab initio calculations to produce accurate results.[39,55] The trial-and-error approach may not accurately represent the adsorption process, whereas ab initio calculations are very computationally expensive.

In this work, we show the accuracy of GCMC simulations for predicting van der Waals interactions from O_2/N_2 adsorption in MOFs and to use the simulation results to better understand the nonbinding interactions that take place between these adsorbates and OMS MOFs. Additional considerations are given to boosting the computational efficiency of Monte Carlo simulations for ambient O_2/N_2 separation screening purposes. The presence of partial charges is shown to have a negligible impact on adsorption at low pressure. Selectivity is calculated using the O_2/N_2 ratio of Henry's constants (referred to as "simple selectivity"), Ideal Adsorbed Solution Theory (IAST), and binary O_2/N_2 adsorption simulations in order to make suggestions for large-scale screening purposes.

2. METHODS

2.1. Selected MOF Structures. Simulations were executed on a variety of Zn-MOFs to assess the role of pore features such as pore diameter and surface area on adsorption properties. The isoreticular MOF series was chosen to systematically observe how interpenetration and the choice of ligand can be used to optimize equilibrium effects of the adsorptive separation of O_2/N_2 mixtures. IRMOF-1 (also called MOF-5) is the prototype for the IRMOF series. Its structure with Zn metal clusters connected by 6 BDC linkers which connect 2 clusters per linker results in a cubic crystal system as displayed in Figure 1 (left). The IRMOFs contain oxide-centered tetrahedral Zn_4O clusters with octahedral secondary building units (SBUs). Each MOF in this series has identical framework topology, making it possible to analyze how structure interpenetration and ligand modifications can be used to optimize selectivity toward O_2. Detailed structural information on the IRMOFs explored in this work are provided in Table 3. IRMOF-3, -4, -5, -6, and -7 contain amine, propoxy, and pentoxy; fused cyclobutyl; and fused benzene groups attached to the carboxylate ligands, respectively, wherein the groups point into the voids of the MOF. IRMOF-9 through -16 contain longer ligand lengths to produce expanded pores, where the odd numbered IRMOFs (i.e., IRMOF-9, -11, -13, and -15) are interpenetrated analogs of the even numbered IRMOFs. Additional simulations were performed on MOF-177 to verify consistency with experiments. MOF-177 also contains 6-coordinated Zn_4O metal clusters which form octahedral SBUs, but each BTB ligand is attached to three metal clusters resulting in a trigonal structure, as shown in Figure 1 (right). The MOFs with SMSs under investigation have a similar synthesis routes as described by Koh et al.[56]

These MOFs were chosen in order to avoid computational inaccuracies caused by the presence of OMSs. A brief comparison of experimental/simulation data for HKUST-1(Cu) and UiO-66 is used to justify the decision. MOF-177 simulations are compared to experimental results to show the accuracy of the generic force fields in describing the O_2/N_2 equilibrium adsorption from dispersion forces in MOFs.

2.2. Computational Details. RASPA molecular software was used to execute Monte Carlo simulations to probe the structure and adsorption properties of the frameworks.[57,58] The Lennard-Jones 6-12 (LJ) force field was used to model the van der Waals interaction of the atoms, as shown in eq 2.

$$E_{vdw} = \varepsilon_{IJ}\left[-2\left(\frac{\sigma_{IJ}}{r}\right)^6 - \left(\frac{\sigma_{IJ}}{r}\right)^{12}\right] \quad (1)$$

The Lorentz−Berthelot mixing rule was used for these interactions, hence the IJ subscript represents the arithmetic mean between a set of parameters. ε_{IJ} [K] is the potential well depth, σ_{IJ} [Å] is the minimum bond length, and r [Å] is the distance between the two atoms. The MOF structures were treated as rigid by fixing their crystallographic coordinates. The crystal structures of selected MOFs were obtained from previous reported structural studies. The crystallographic coordinates for the IRMOF series were obtained from Eddaoudi et al.[59] MOF-177 coordinates were included in the RASPA software by Dubbeldam et al.[57] UiO-66 and HKUST-1(Cu) coordinates were taken from the literature, as well.[60,61] Lennard-Jones parameters from the Universal Force Field were applied to the metal ions,[62] whereas values were taken from the DREIDING force field for other frameworks atoms.[63] Solvent molecules were not included in the crystallographic information in order to represent the activated samples. O_2 and N_2 were modeled as rigid bodies using the three-site model from the TraPPE force field.[64] A table of the Lennard-Jones parameters used are summarized in Table S1. To avoid the double-counting problem, cubic simulation boxes with dimensions equal to their respective unit cell were used for all MOFs except UiO-66 and IRMOF-9; for these, simulation box dimensions were 41.4 × 41.4 × 41.4 Å^3 and 34.3 × 46.6 × 25.3 Å^3, respectively, to ensure that the simulation boxes were twice the cutoff distance of 12 Å. Coulombic interactions were modeled by the Ewald summation of point charges. Partial charges were obtained via the extended ChargeEQ equilibration method[47] and are listed in Table S2. The Ewald precision was set to 10^{-6}. Insertion, deletion, translation, and rotation moves were performed with equal probability for 10^6 cycles. Equilibrium was determined to have been reached by verifying that the acceptance ratio of swap addition and swap deletion were nearly equal. Heats of adsorption were calculated by the GCMC method proposed by Vuong and Monson.[65] The focus of this study is MOFs for ambient O_2/N_2 separation, so the

DOI: 10.1021/acs.iecr.8b00981
Ind. Eng. Chem. Res. 2018, 57, 9240−9253

simulations were executed at 298 K for five pressure values up to 1 bar.

Monte Carlo simulations offer a fast method of screening for desirable pore structures and adsorption properties with a minimal amount of resources. Gas separation studies generally report the adsorption uptake as the excess adsorption, which is defined as the amount of gas present beyond the bulk fluid phase under the experimental conditions. Excess adsorption is expressed as

$$n^{ex} = n^{abs} - V^g \rho^g \quad (2)$$

where n^{abs} is the absolute amount adsorbed (mol/kg), V^g is the pore volume of the framework (cm^3/kg), and ρ^g (mol/cm^3) is the bulk density of the gas phase. In order to compare simulation and experimental results, pore volumes were determined from a computational technique that was developed to mimic the experimental method using helium probe molecules.[66] Accessible surface areas were determined using the methods proposed by Duren et al.[67] In this technique, the surface area of the input structure is measured using a probe molecule rolling over the entire surface of the pore walls.[57] N_2 was used as the probe molecule for determining the accessible surface area in this study because it has the larger diameter of the two gases under investigation. Pore size distributions were determined using the method proposed by Gelb and Gubbins.[68] The pore size distribution is determined by finding the largest sphere that can be generated without overlapping with framework atoms at each point in the void space. The coverable volume for a particular sphere radius, denoted as $V_{pore}(r)$, can then be determined and compared to cumulative pore volume curves from experiments.

3. RESULTS

3.1. Simulation/Experimental Comparison of Isotherms for MOFs with Exposed, Nonbinding Metal Sites. N_2-selective samples of HKUST-1(Cu) have been produced by multiple groups,[26,27,37] but GCMC simulations using generic force fields did not predict the selectivity toward N_2, as shown in Figure 2. The N_2 isotherm was predicted accurately, but the O_2 isotherm was highly overestimated, leading to the inability of the simulations to predict nitrogen selectivity.

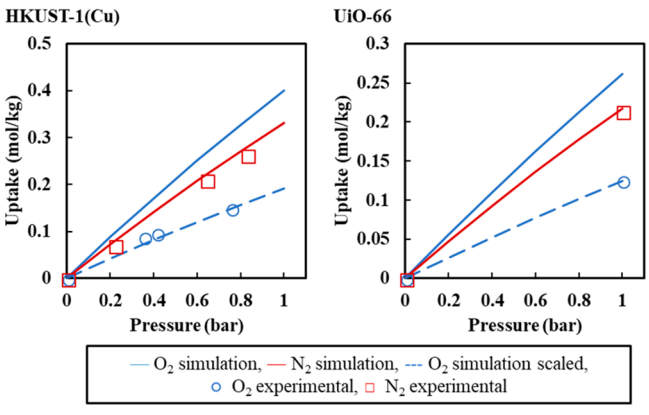

Figure 2. Comparison of HKUST-1(Cu) (left) and UiO-66 (right) simulated O_2/N_2 isotherms with experimental data and 47.7% scaled O_2 simulation isotherms. HKUST-1(Cu) experimental data are from Wang et al.,[57] and UiO-66 experimental data are from Piscopo et al.[17]

GCMC simulations using generic force fields also significantly overpredicted the O_2 isotherm of UiO-66 (Figure 2), which is attributed their synthesis procedure generating OMSs. Scaling the O_2 uptake by 47.7% leads to highly accurate prediction in both cases, indicating the existence of an interaction that is not captured by generic force fields. Due to the inability of generic force fields to describe O_2 adsorption at OMSs, MOFs with saturate metal sites were the focus of the remainder of the study.

3.2. Model Verification and Simplification. *3.2.1. Structural Model Verification for IRMOF Series.* Simulations were executed on a variety of Zn-MOFs to assess the effects of pore features on adsorption properties. These MOFs include IRMOF-1, IRMOF-3, IRMOF-4, IRMOF-5, IRMOF-6, IRMOF-7, IRMOF-9, IRMOF-10, IRMOF-11, IRMOF-12, IRMOF-13, IRMOF-14, IRMOF-15, IRMOF-16, and MOF-177. The first phase of simulations was performed to determine the surface area, pore volumes, and pore size distribution of a large number frameworks to ensure that the conclusions drawn from this study are generalizable. At the low pressures of interest, the adsorption is expected to be impacted mainly by pore size because surface saturation and pore filling effects do not come into play. The calculated accessible surface areas and distinct pores are displayed and compared to reported values in Table 4.

As shown in Table 4, the selected structures have surface areas ranging from less than 1000 to over 6000 m^2/g, pore volumes from 0.375 to 2.24 cm^3/g, and distinct pore from 3.50 to 24.2 Å. IRMOF structures have been studied extensively, and the calculated pore features are in good agreement with literature.[59,67]

3.2.2. Force Field Verification by Comparison of MOF-177 Simulation Results with Experiments. Simulations were performed on MOF-177 to verify that the simulation results match with experiments. First, experimentally determined pore features are compared against the simulated data in Table 5 to verify the structural model for MOF-177. In the low-pressure regime, adsorption is expected to be impacted primarily by the pore size. Because the pore sizes match perfectly, the GCMC adsorption results can be compared to the experiments to show the accuracy of predicting van der Waals interactions. From Figure 3, it is clear the van der Waals interactions are properly represented by the generic force fields.

3.2.3. Presence of Charge Does not Impact O_2/N_2 Adsorption at Low Pressure. As indicated by other groups,[27,55] there appears to be a negligible impact of electrostatic interactions on uptake of O_2 and N_2 at low pressures. A comparison of isotherms with and without charges for IRMOF-1 and MOF-177 are shown to be virtually indistinguishable in Figure S1. This implies that polarity does not impact adsorption of these gases onto MOFs with SMSs under ambient conditions. The lack of a need for an accurate charge equilibration technique makes large scale screening of MOFs for ambient air separation possible with a low computational cost.

3.2.4. O_2/N_2 Mixed Gas Simulations, IAST Calculations, and Simple Selectivity Calculations. Four methods of determining mixed gas selectivity which vary in computational complexity were used: the ratio of K_H values from pure gas isotherms (referred to as "simple" selectivity), IAST calculations from Henry's law fitted isotherms, IAST calculations from dual-site Langmuir–Freundlich fitted isotherms, and binary O_2/N_2 adsorption simulations. Simple selectivity

DOI: 10.1021/acs.iecr.8b00981
Ind. Eng. Chem. Res. 2018, 57, 9240–9253

Table 4. Pore Features of IRMOFs Compared to Duren et al.[55]

	this work	Duren et al.	this work	Duren et al.
IRMOF-1	3686	3580	11.1/14.6	10.9/14.3
IRMOF-3	3494		9.4/14.5	
IRMOF-4	1647		4.1/4.4/7.3/9.1	
IRMOF-5	956		6.8/8.1/9.6	
IRMOF-6	3180	3050	9.4/14.5	9.1/14.3
IRMOF-7	3487		10.4	
IRMOF-9	3592	4017	4.6/6.5/8.2/10.8	4.6/6.5/8.3/10.8
IRMOF-10	4693		16.9/20.2	16.7/20.2
IRMOF-11	2753	2702	3.5/4.0/4.6/6.1/6.7/11.8	3.5/3.8/4.7/6.1/7.0/11.1
IRMOF-12	5237		14.7/18.5	
IRMOF-13	2835	2998	4.2/4.7/6.5/8.3/10.9	4.2/4.7/6.1/7.0/11.4
IRMOF-14	4844	4926	14.8/20.0	14.1/19.5
IRMOF-15	2498		7.3/9.5	
IRMOF-16	6046	6166	24.2	23.3

Table 5. Comparison of Predicted MOF-177 Pore Features with Experimental Values from Dipendu et al.[15]

	surface area [m^2/g]	available pore volume [cm^3/g]	average pore diameter [Å]
simulated	4850	1.97	10.6
experimental	3100	1.58	10.6

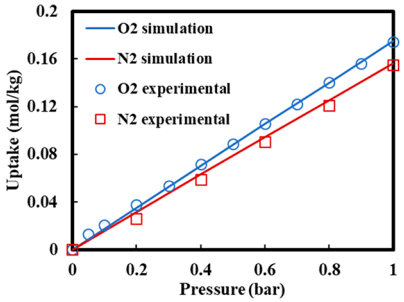

Figure 3. Comparison of MOF-177 simulated O_2/N_2 isotherms with experimental data. O_2 experimental data are from Li et al.,[15] and N_2 experimental data are from Dipendu et al.[16]

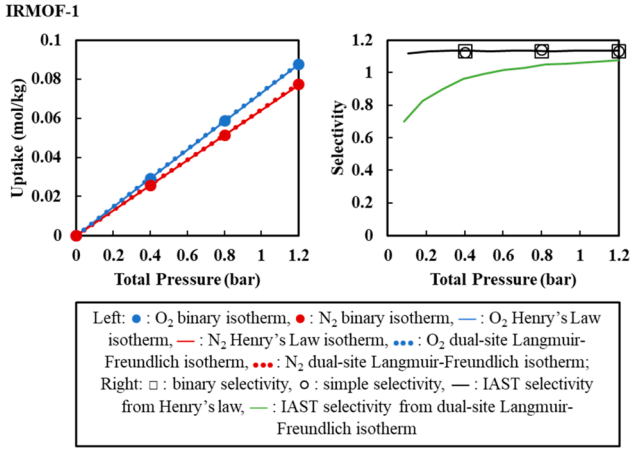

Figure 4. Left: comparison binary gas isotherms, Henry's Law fitted pure isotherms, and dual-site Langmuir–Freundlich fitted isotherms; right: comparison of binary gas selectivity with simple selectivity (ratio of K_H values), IAST selectivity calculated from Henry's law fitted isotherms, and IAST selectivity calculated from dual-site Langmuir–Freundlich fitted isotherms.

calculations offer a fast method of estimating the mixed gas selectivity, which are expected be accurate at low pressure. IAST calculations have been widely used to describe mixed gas interactions.[3,7,69] It is common to fit the pure gas isotherms to the dual-site Langmuir–Freundlich equation in IAST calculations;[69] however, more accurate results have been achieved using Henry's law when the low loading (and low pressure) region is being investigated.[70] IAST selectivity was calculated using both Henry's law and the dual-site Langmuir–Freundlich equation to compare results.

The binary gas isotherm for IRMOF-1 is compared to the fitted isotherms in Figure 4 (left), where the fitted isotherms are treated as individual pure gas terms for the binary system. The pure isotherms and their fitted equations are in excellent agreement with the binary gas simulation isotherms. The binary gas selectivity is plotted with the simple selectivity and IAST selectivity using both isotherm fits in Figure 4 (right). The IAST calculations using the dual-site Langmuir–Freundlich equation is not in good agreement with the binary gas selectivity calculation at low pressure, which can be attributed to lack of precision in describing the low-pressure data caused by the need for the equation to describe the high-pressure region. Since the dual-site Langmuir–Freundlich fitted isotherm appears to match the binary adsorption data well but there are errors in the IAST selectivity, it can be concluded that the IAST selectivity is sensitive to small differences in the isotherm fit. The IAST calculations using Henry's law, on the other hand, are in excellent agreement with the binary gas selectivity data. The simple selectivity calculations appear to accurately predict the adsorption of mixed gas systems at the low pressures of interest, which greatly reduces the computational cost of understanding the adsorption of the O_2/N_2 binary system. Mixed gas adsorption simulations are computationally expensive, but this shows that the selectivity of the binary system could be determined in other ways.

3.3. Influence of Pore Features on Ambient O_2/N_2 Adsorption. *3.3.1. Ligand Substituent Groups.* Figures 5–9 show the adsorption isotherms, IAST selectivities, and pore size distributions of the MOFs under investigation. The same information was generated for MOF-177, but this is included in Figure S2 because it has a relatively undesirable pore diameter, making it relatively inert for air separation applications. IRMOF-1 has two distinct pores at 11.1 and 14.6 Å. It has a relatively low Henry's constant (K_H) for both O_2 and N_2 less than 0.15 mol/kg bar. The IAST selectivity is

DOI: 10.1021/acs.iecr.8b00981
Ind. Eng. Chem. Res. 2018, 57, 9240–9253

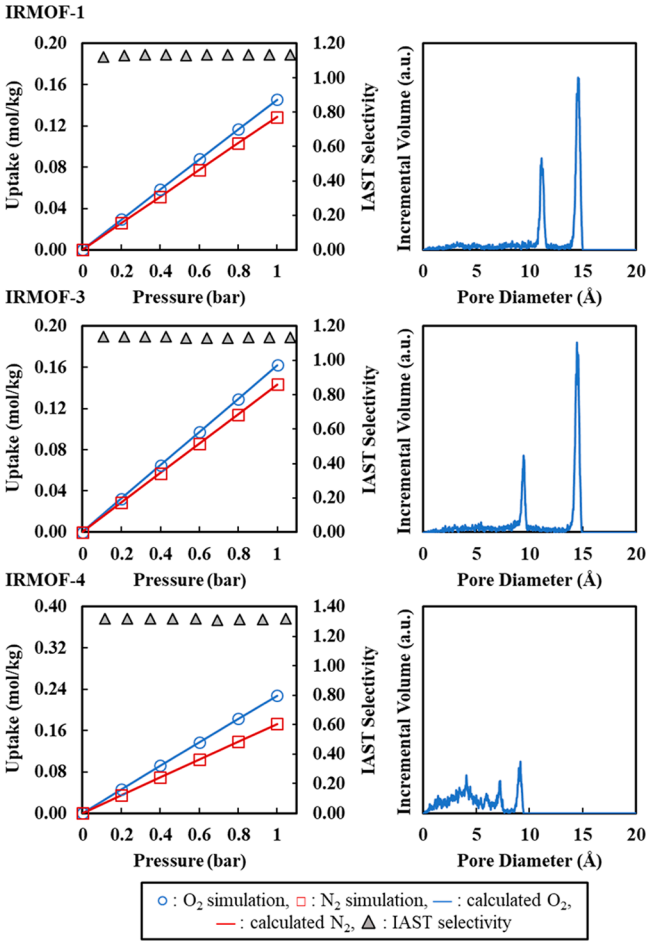

Figure 5. O_2/N_2 adsorption isotherms (left); simulated pore size distribution (right).

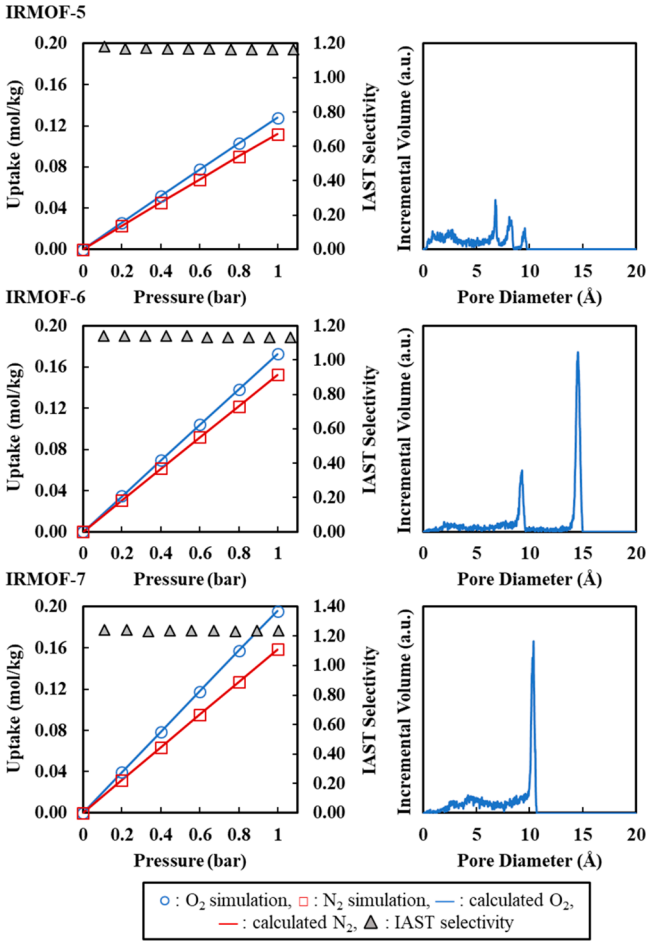

Figure 6. O_2/N_2 adsorption isotherms (left); simulated pore size distribution (right).

essentially constant at 1.13 as the pressure increase from 0.05 to 1 bar.

Adding an amine group to the carboxylate ligand (IRMOF-3) results in reduced pore sizes of 9.4 and 14.5 Å. The adsorption isotherms and IAST selectivity are virtually unaffected by the change. The addition of a propoxy group (IRMOF-4) results in a broader distribution of pore sizes with local maxima at 4.1 and 9.1 Å. This change results in a noticeable increase in K_H for O_2 to 0.22 mol/kg bar and N_2 to 0.17 mol/kg bar. The IAST selectivity was constant at 1.32 from 0.05 to 1 bar. If the functional group is extended to a pentoxy group (IRMOF-5), there is a distribution of pores from 0 to 10 Å with local maxima at 6.8, 8.1, and 9.7 Å. Both K_H values are reduced to below 0.13 mol/kg bar with IAST selectivity relatively constant at 1.17 bar. The inclusion of a fused cyclobutyl group in the ligand (IRMOF-6) results in a pore size distribution almost identical to IRMOF-3, again with a minimal effect on the adsorption capacity of N_2 and O_2 with a constant IAST selectivity of 1.13. The addition of a fused benzene group (IRMOF-7) results in a structure with one distinct pore at 10.4 Å. Both N_2 and O_2 uptakes are larger than that of IRMOF-1, and the selectivity is constant at 1.24 from 0.2 to 1 bar.

Ligand functionalization clearly can result in complex pore size distributions. For IRMOF-3 and -6, the two pores of IRMOF-1 were slightly reduced. In IRMOF-7, there was only 1 distinct pore smaller than either pore in IRMOF-1, resulting in an increased O_2/N_2 selectivity. The addition of alkoxy groups (IRMOF-4 and -5) results in a broad distribution of pores from 0 to 10 Å. The pore sizes less than 3.46 Å can be neglected because the gases of interest cannot diffuse through these pores. The enhanced uptake and selectivity of IRMOF-4 can be attributed to the broad pore distribution that peaks at 4.1 Å. Although there appears to be pores from 3.46 to5.00 Å in IRMOF-5, the major pores are all greater than 6.8 Å.

3.3.2. Ligand length. The O_2/N_2 adsorption isotherms and IAST selectivities of IRMOF-9 through -16 are displayed in Figures 7–9. The BPDC and TPDC ligand of IRMOF-10 and -16, respectively, can be thought of as extended BDC ligands. IRMOF-10 has two distinct pores at 14.8 and 20.2 Å, whereas IRMOF-16 has one pore at 24.2 Å. IRMOF-10 and -16 both have a slight increase in uptake of both gases but constant selectivity of 1.13, similar to IRMOF-1. This shows that (1) high pore volumes and surface areas have a minimal effect on selectivity and (2) pore diameters larger than IRMOF-1 are past the region in which selectivity is enhanced by small pore size.

3.3.3. Interpenetrated Structures. There are four sets of interpenetrated/noninterpenetrated structures to compare: IRMOF-9 and -10; -11 and -12; -13 and -14; and -15 and -16. IRMOF-9, the interpenetrated form of IRMOF-10, has a relatively broad pore size distribution, with local maxima at 4.6, 6.5, 8.2, and 10.8 Å. The significant reduction in pore size results in a substantial increase in uptake of both O_2 and N_2.

DOI: 10.1021/acs.iecr.8b00981
Ind. Eng. Chem. Res. 2018, 57, 9240–9253

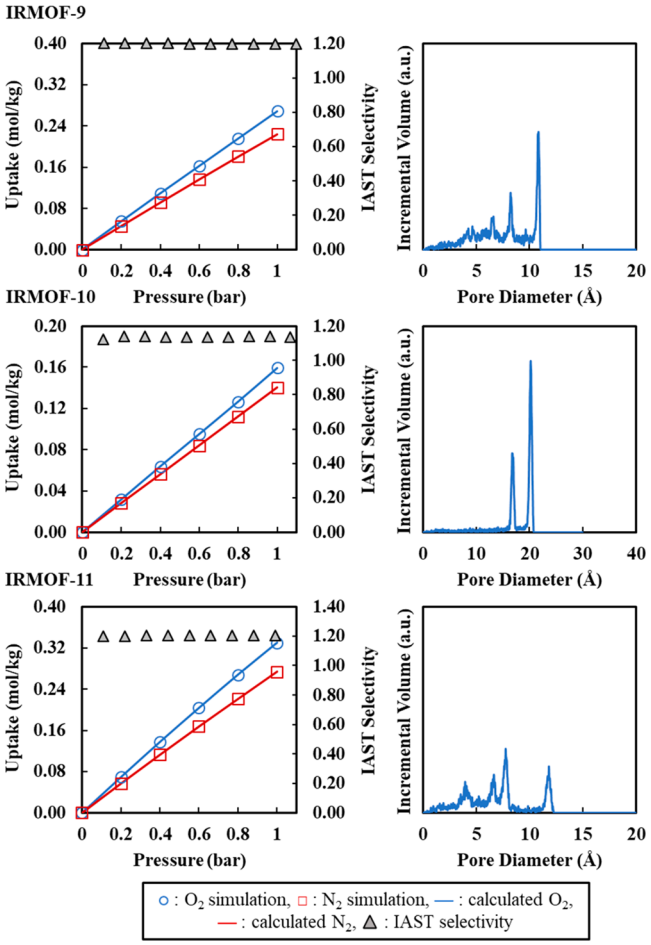

Figure 7. O_2/N_2 adsorption isotherms (left); simulated pore size distribution (right).

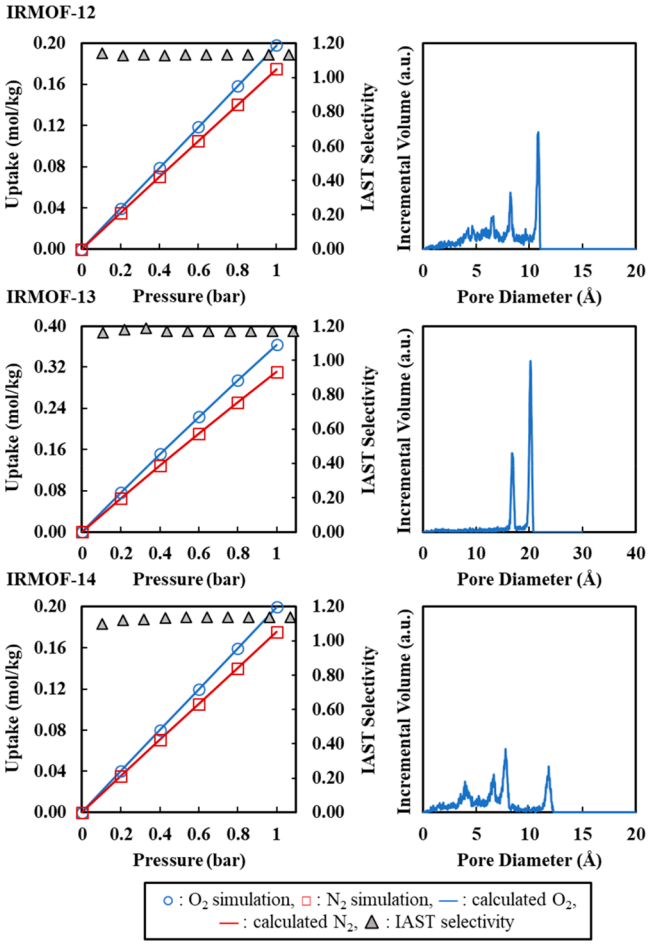

Figure 8. O_2/N_2 adsorption isotherms (left); simulated pore size distribution (right).

The K_H values increase from 0.159 to 0.268 mol/kg bar for O_2 and from 0.140 to 0.224 mol/kg bar for N_2. The IAST selectivity of IRMOF-9 is constant at 1.20 from 0.05 to 1 bar, a significant improvement from IRMOF-10. IRMOF-12 has slightly smaller pore sizes compared to IRMOF-10 with distinct pores at 14.7 and 18.5 Å. The interpenetrated IRMOF-11 has broad distribution of pores similar to IRMOF-9, with peaks at 3.5, 3.9, 4.6, 6.7, 7.8, and 11.8 Å. For IRMOF-11, the K_H values of O_2 and N_2 are 0.33 and 0.274 mol/kg bar, respectively, resulting in a constant selectivity of 1.20 from 0.05 to 1 bar. The selectivity of its noninterpenetrated counterpart, IRMOF-12, is constant at 1.13 from 0.05 to 1 bar. IRMOF-14 has larger pores than IRMOF-12 with distinct pores at 14.8 and 20.0 Å. The IAST selectivity is constant at 1.13 from 0.05 to 1 bar. The interpenetrated analog, IRMOF-13, has a broad pore size distribution with a large peak at 11.4 Å and smaller peaks at 4.2, 4.7, 6.1, and 7.0 Å. The K_H value of O_2 is increased from 0.20 to 0.363 mol/kg bar and N_2 from 0.175 to 0.311 mol/kg bar, resulting in a selectivity of 1.17 from 0.05 to 1 bar. IRMOF 15, the interpenetrated structure with the longest ligand, has a distribution of pore from 7 to 10 Å with peaks at 7.3 and 9.5 Å. The K_H values are low compared to other interpenetrated MOFs: K_H = 0.186 mol/kg bar for O_2 and K_H = 0.169 mol/kg bar for N_2. The selectivity of IRMOF-15 is 1.11 from 0.05 to 1 bar.

Interpenetrated structures result in a large increase in uptake and selectivity if pore diameters approaching the molecular

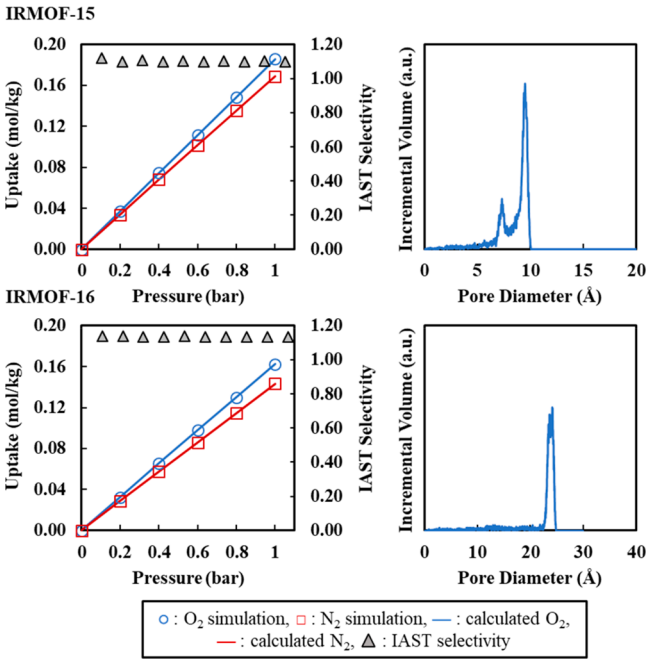

Figure 9. O_2/N_2 adsorption isotherms (left); simulated pore size distribution (right).

DOI: 10.1021/acs.iecr.8b00981
Ind. Eng. Chem. Res. 2018, 57, 9240−9253

diameter of the gases of interest are generated. The IAST selectivity of each of the interpenetrated MOFs with subnanopores converged to around 1.2. This is likely because of the similar ligand length and pore size distributions of these structures. The similar selectivities of IRMOF-12 and -14 to IRMOF-1 is consistent with the notion that ligand lengths larger than IRMOF-1 will not enhance selectivity toward oxygen.

4. DISCUSSION

4.1. GCMC Model Inaccuracies for MOFs with Open Metal Sites. The HKUST-1 and UiO-66 samples analyzed both have N_2/O_2 selectivities of 1.7 based on previous experiments, but GCMC simulations using generic force fields did not predict the nitrogen selectivity. Attempts at increasing the selectivity toward nitrogen could make MOFs competitive with zeolites commonly used for medical oxygen concentrators. This is just one reason why it is important to understand the mechanism that results in N_2-selective adsorption in MOFs.

As demonstrated, GCMC simulations significantly overpredicted the O_2 adsorption in HKUST-1(Cu) and UiO-66. In both cases, scaling the O_2 isotherm by 47.7% results in a very accurate predicted isotherm as compared with experiments. Inaccurate prediction of O_2 isotherms in MOFs with nonbinding metal sites implies that there is a nondispersion interaction that comes into play in OMS MOFs, even when the metal sites do not chemisorb oxygen. While we cannot give a detailed explanation based on our results, it is a relevant topic to this discussion that could lead to future work. As such, we now would like to relate it to observations from previous groups.

This finding is consistent with the work of Sava Gallis et al., who experimentally observed higher heats of adsorption for N_2 compared to O_2 in mixed metal variants of HKUST-1.[27] Their experimental heat of adsorption data for N_2 on HKUST-1(Cu) matches perfectly with our value of 14.7 kJ/mol from simulations, whereas their value for O_2 of 10.7 kJ/mol is only a fraction of the simulation value of 15.0 kJ/mol. They also reported a much higher heat of adsorption of N_2 in the Fe-substituted sample with a +3 oxidation state, which may suggest that the unknown interaction is electrostatic in nature. These interesting phenomena which are not predicted by GCMC simulations may be related to the short-range physical interactions previously observed between methane and HKUST-1(Cu) in the neutron diffraction study from Getzschmann et al.;[54] importantly, they suggest this is caused by the Lewis acidity of the OMS polarizing the otherwise nonpolar CH_4 molecule.[54] To be clear, these interactions are similar because they are not predicted by GCMC simulations, they are too weak to be caused by chemisorption, they are exclusive to OMS MOFs, and current data are consistent with electrostatic interactions.

4.2. Suggested Multiphase Screening Method. In the following sections we investigate adsorbate interactions as a function of pore diameter and suggest future simulation work. However, first, we find it important to summarize key findings that minimize the computational cost of GCMC simulations on this topic.

The simulated isotherms were shown to be unaffected by partial charges at the low pressures under investigation. Mixed gas adsorption simulations were demonstrated to be unnecessary due to the accuracy of IAST selectivity calculations. Simple selectivity calculations can even be used to accurately estimate of selectivity up to 1 bar. With these insights, screening for desirable van der Waals interactions in MOFs for ambient O_2/N_2 can be accurately performed with low computational cost.

4.3. Volume-Weighted Average Accessible Pore Diameter Definition. IAST selectivity for each of the materials do not correlate well with surface area or pore volume because surface saturation and pore filling usually do not come into play under the conditions of interest. On the other hand, a clear relationship can be seen between the IAST selectivity and pore size. Due to the complex pore size distribution of many MOFs, it can be difficult to see how the pore size affects the adsorption properties. The volume-weighted average accessible (VWAA) pore diameter, as defined below, can be used to capture the pore size distribution into a single parameter by weighting the average diameter with the fraction of coverable volume for a particular sphere radius.

$$d_{av} = \sum_{i=1}^{i} \frac{V_{pore}^{i}}{\sum_{i=1}^{i} V_{pore}^{i}} d_i \tag{3}$$

where d_{av} is the VWAA pore diameter and d_i is the pore diameter associated with the coverable volume V_{pore}^{i}. The index term, i, should start at the pore size of the smallest diameter gas of interest because smaller pores are inaccessible to the gases. The IAST selectivity is plotted as a function of VWAA pore diameter and mode pore diameter in Figure S3 (top) to show the substantially improved correlation. Our research group is unaware of anyone using such a definition for the average pore diameter to accurately represent broad pore size distributions. The downfall of this method of representing the data is that information about distinct pores is lost, making it difficult to apply for characterization purposes. For example, the overlap of the MOF-177 simulated and experimental O_2 uptake vs mode pore diameter data points in Figure S3 (bottom) demonstrates the accuracy of Monte Carlo simulations in predicting these properties, but the same graph as a function of VWAA pore diameter could not be generated because most groups only report the distinct pores.

This parameter could be useful for understanding the correlation between pore diameter and adsorption properties in real-world materials beyond the scope of this study. We obtained much clearer correlations using this parameter instead of the mode pore diameter to study equilibrium adsorption.

4.4. Adsorbent−Adsorbate Interactions as a Function of VWAA Pore Diameter. The adsorbate−adsorbate interactions are negligible for all simulations executed in this study, which makes the adsorbent−adsorbate interaction equal in magnitude to the heats of adsorption for each simulation. The adsorbent−adsorbate interactions are essentially constant from 0.2 to 1 bar for all MOFs. As shown in Figure 10 (top) the adsorbent−adsorbate interactions for both O_2 and N_2 are enhanced by lower pore diameters. As the pore diameter approaches the molecular diameter of oxygen, surfaces are interacting with the molecules from multiple directions, causing a substantially higher affinity of the adsorbate to the material. Enhanced pore wall interactions have been described elsewhere at low pressure for CO_2/CH_4 separation.[48] The enhanced selectivities result from a slightly larger increase in adsorbent−adsorbate interaction for O_2.

DOI: 10.1021/acs.iecr.8b00981
Ind. Eng. Chem. Res. 2018, 57, 9240−9253

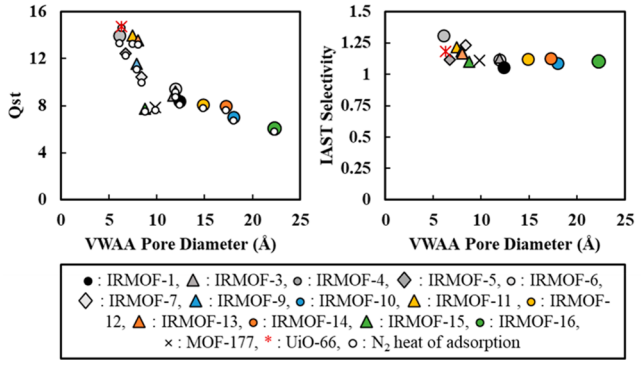

Figure 10. IAST selectivity and heat of adsorption as a function of volume-weighted average accessible pore diameter.

A direct comparison of our results to those of Greathouse et al.[35] in terms of heat of adsorption shows that the MOFs studied here are still well outside the range in which substantially improved selectivity would be expected. The heat of adsorption of both gases in their largest diameter nanotube (5.07 Å) is 15−16 kJ/mol, slightly larger than the range of 14−15 kJ/mol observed in our simulations with VWAA pore diameters near 5.97 Å. This is promising for future work on this topic because it allows us to set goals for understanding the selectivity that can be achieved for O_2/N_2 separation via this mechanism. Because it is already known that the maximum heats of adsorption can be achieved near 4.5 Å, this should be the target for VWAA pore diameter of materials to achieve the maximum equilibrium adsorption or the two adsorbates. The biggest difference in heats of adsorption between O_2 and N_2 occurs around 3.38 Å, so this should be the target to achieve the highest selectivity.

4.5. IAST Selectivity as a Function of VWAA Pore Diameter. Figure 10 (bottom) shows a summary of the data generated in this study. There is a clear correlation between IAST selectivity at 1 bar and VWAA pore diameter. As shown, the enhanced selectivity that results from smaller pore sizes applies to pores less than about 8 Å. When pore diameters are larger than this, the selectivity converges to about 1.1 at 1 bar. The success of establishing a correlation between the selectivity and this parameter suggests that the adsorption is not affected by the existence of broad vs distinct pores, as long as pores less than 8 Å make up a large portion of the free volume. The smallest VWAA pore diameter of the samples investigated is 5.97 Å. Although this is only about a 20% increase compared to unenhanced MOFs, the principle can be exploited to further improve the selectivity. The selectivity toward oxygen is expected to improve even more dramatically with pore sizes ranging from 3.38 to 4.50 Å based on the heat of adsorption results from Greathouse et al.,[35] so this should be the target for future work in developing O_2-selective materials based on this mechanism.

The addition of substituent groups can be used as a tool to reduce the pore size and enhance O_2/N_2 selectivity, but it is difficult to predict how the pore size distribution will be changed. Interpenetration, on the other hand, seems to generate small pores in a more consistent manner if nanopores already exist within the framework. The combination of these two techniques may be a promising way of further improving the selectivity toward oxygen.

5. CONCLUSIONS

There are multiple mechanisms to achieve separation of O_2/N_2 mixtures in MOFs, which introduces opportunities for exploiting these mechanisms and challenges to the rational design for specific applications. MOFs previously studied for ambient air separation were categorized based on the presence of OMSs and the oxygen-binding activity of the metal sites to better understand the dominant interactions that come into play in various MOF structures. It is clear that SMS MOFs selectively physisorb oxygen based on dispersion forces and MOFs with binding metal sites selectively chemisorb oxygen. We showed that the exposed, nonbinding metal sites of HKUST-1(Cu) and UiO-66 result in a substantial decrease in O_2 uptake that cannot be predicted by GCMC simulations, which suggests that there is another nonbinding interaction occurring at the metal sites. This finding was compared to similar results in literature on adsorption at OMS and conclude that it is likely an electrostatic interaction caused by the presence of OMS. Future work on this topic should be aimed at characterizing these interactions and understanding how they can be exploited in MOFs for air separation, as well as for other applications.

The accuracy of Monte Carlo simulations for predicting pore features and equilibrium adsorption from van der Waals interactions in MOFs was demonstrated by comparison of experiments with MOF-177. Consideration was given to ways of improving the efficiency of the simulations for large-scale screening purposes. The low-pressure adsorption results appear to be unaffected by the presence of electrostatic charges, making concerns over charge equilibration irrelevant. IAST selectivities and simple selectivities were shown to match well with binary O_2/N_2 mixed gas GCMC adsorption simulations. A multiphase screening technique specific to ambient O_2/N_2 separation was suggested to simplify future simulation work in this area.

The VWAA pore diameter, as defined in this paper, was suggested to represent the pore size distribution in a single parameter to establish a clear correlation with adsorptive properties and to relate the work of Greathouse et al. on idealized CNTs[35] to more complex pore size distributions. We showed improved selectivity in MOFs with VWAA pore diameters less than 8 Å going from 1.1 to 1.3 at a diameter of 5.97 Å. While this is still larger than the pore diameters investigated in the nanotube study (the highest being 5.07 Å), our closest data points are in good agreement (14−15 and 15−16 kJ/mol, respectively). It is promising that increased selectivity was observed at pore diameters significantly greater than those that can be attributed to the highest adsorbent−adsorbate interactions and selectivity in CNT systems. Future work should use the suggested screening method to identify or design MOFs with VWAA pore diameters at target values of 4.50 and 3.38 Å in which the maximum heats of adsorption and maximum difference in heats of adsorption are achieved for an O_2/N_2 system, respectively. Similar correlations using other materials and gases will also likely give fruitful results in comparing different porous adsorbents and the impact of pore heterogeneity on equilibrium adsorption.

■ ASSOCIATED CONTENT

Supporting Information

The Supporting Information is available free of charge on the ACS Publications website at DOI: 10.1021/acs.iecr.8b00981.

DOI: 10.1021/acs.iecr.8b00981
Ind. Eng. Chem. Res. 2018, 57, 9240−9253

Table of Lennard-Jones Parameters used in GCMC simulations (Table S1), simulated adsorption isotherms for IRMOF-1 and MOF-177 with and without charges (Figure S1), table of partial charges used in simulations (Table S2), MOF-177 simulated adsorption isotherm and pore size distribution (Figure S2), and comparison of VWAA pore diameter correlations with mode pore diameter (Figure S3) (PDF)

AUTHOR INFORMATION

Corresponding Authors

*E-mail liujc@ecust.edu.cn.
*E-mail bmu@asu.edu.

ORCID

Bohan Shan: 0000-0001-5674-981X
Jichang Liu: 0000-0002-5295-1778
Bin Mu: 0000-0002-9117-1299

Author Contributions

§Co-first authors.

Notes

The authors declare no competing financial interest.

ACKNOWLEDGMENTS

S.M. was supported by the NASA Space Grant Undergraduate Research Fellowship for this project. B.M. acknowledges the National Science Foundation (Grant Number CBET-1748641). J.L. was supported by the National Natural Science Foundation of China (Project 21476082). We also gratefully acknowledge the use of computing resources from ASU Research Computing Center.

REFERENCES

(1) Li, J. R.; Sculley, J.; Zhou, H. C. Metal-Organic Frameworks for Separations. *Chem. Rev.* **2012**, *112* (2), 869−932.
(2) Herm, Z. R.; Bloch, E. D.; Long, J. R. Hydrocarbon Separations in Metal-Organic Frameworks. *Chem. Mater.* **2014**, *26* (1), 323−338.
(3) Mu, B.; Li, F.; Walton, K. S. A Novel Metal−organic Coordination Polymer for Selective Adsorption of CO2 over CH4. *Chem. Commun.* **2009**, *18*, 2493.
(4) Mu, B.; Walton, K. S. Adsorption Equilibrium of Methane and Carbon Dioxide on Porous Metal-Organic Framework Zn-BTB. *Adsorption* **2011**, *17* (5), 777−782.
(5) Mu, B.; Schoenecker, P. M.; Walton, K. S. Gas Adsorption Study on Mesoporous Metal-Organic Framework UMCM-1. *J. Phys. Chem. C* **2010**, *114* (14), 6464−6471.
(6) Mu, B.; Li, F.; Huang, Y.; Walton, K. S. Breathing Effects of CO2 Adsorption on a Flexible 3D Lanthanide Metal−organic Framework. *J. Mater. Chem.* **2012**, *22* (20), 10172.
(7) Shan, B.; Yu, J.; Armstrong, M. R.; Wang, D.; Mu, B.; Cheng, Z.; Liu, J. A Cobalt Metal-Organic Framework with Small Pore Size for Adsorptive Separation of CO2 over N2 and CH4. *AIChE J.* **2017**, *63* (10), 4532−4540.
(8) Zhou, W. Methane Storage in Porous Metal−organic Frameworks: Current Records and Future Perspectives. *Chem. Rec.* **2010**, *10* (3), 200−204.
(9) Armstrong, M. R.; Shan, B.; Cheng, Z.; Wang, D.; Liu, J.; Mu, B. Adsorption and Diffusion of Carbon Dioxide on the Metal-Organic Framework CuBTB. *Chem. Eng. Sci.* **2017**, *167* (22), 10−17.
(10) Gu, Z.-Y.; Park, J.; Raiff, A.; Wei, Z.; Zhou, H.-C. Metal-Organic Frameworks as Biomimetic Catalysts. *ChemCatChem* **2014**, *6* (1), 67−75.
(11) Chughtai, A. H.; Ahmad, N.; Younus, H. A.; Laypkov, A.; Verpoort, F. Metal−organic Frameworks: Versatile Heterogeneous Catalysts for Efficient Catalytic Organic Transformations. *Chem. Soc. Rev.* **2015**, *44* (19), 6804−6849.
(12) Lustig, W. P.; Mukherjee, S.; Rudd, N. D.; Desai, A. V.; Li, J.; Ghosh, S. K. Metal−organic Frameworks: Functional Luminescent and Photonic Materials for Sensing Applications. *Chem. Soc. Rev.* **2017**, *46* (11), 3242−3285.
(13) Balzer, C. J.; Armstrong, M. R.; Shan, B.; Mu, B. Composite MOF Mixture as Volatile Organic Compound Sensor − A New Approach to LMOF Sensors. *Mater. Lett.* **2017**, *190*, 33−36.
(14) Horcajada, P.; Gref, R.; Baati, T.; Allan, P. K.; Maurin, G.; Couvreur, P.; Férey, G.; Morris, R. E.; Serre, C. Metal-Organic Frameworks in Biomedicine. *Chem. Rev.* **2012**, *112* (2), 1232−1268.
(15) Cunha, D.; Gaudin, C.; Colinet, I.; Horcajada, P.; Maurin, G.; Serre, C. Rationalization of the Entrapping of Bioactive Molecules into a Series of Functionalized Porous Zirconium Terephthalate MOFs. *J. Mater. Chem. B* **2013**, *1* (8), 1101.
(16) Yang, R. T. *Adsorbents: Fundamentals and Applications*; John Wiley & Sons, Inc.: Hoboken, NJ, 2003.
(17) NASA SBIR/STTR Programs. Novel Metal Organic Framework Synthesis for Spacecraft Oxygen Capture.
(18) *NASA STTR 2014 Phase I Solicitation*; NASA: Washington, DC, 2014, 2−3.
(19) *Life Support Systems: On-Board Oxygen Generation Systems (OBOGS)*; Honeywell International Inc., 2008.
(20) Scheffknecht, G.; Al-Makhadmeh, L.; Schnell, U.; Maier, J. Oxy-Fuel Coal Combustion-A Review of the Current State-of-the-Art. *Int. J. Greenhouse Gas Control* **2011**, *5*, 16−35.
(21) Mu, B.; Schoenecker, P. M.; Walton, K. S. Gas Adsorption Study on Mesoporous Metal−Organic Framework UMCM-1. *J. Phys. Chem. C* **2010**, *114* (14), 6464−6471.
(22) Li, Y.; Yang, R. T. Gas Adsorption and Storage in Metal−Organic Framework MOF-177. *Langmuir* **2007**, *23* (26), 12937−12944.
(23) Saha, D.; Bao, Z.; Jia, F.; Deng, S. Adsorption of CO2, CH4, N2O, and N2 on MOF-5, MOF-177, and Zeolite 5A. *Environ. Sci. Technol.* **2010**, *44* (5), 1820−1826.
(24) Piscopo, C. G.; Trapani, F.; Polyzoidis, A.; Schwarzer, M.; Pace, A.; Loebbecke, S. Positive Effect of the Fluorine Moiety on the Oxygen Storage Capacity of UiO-66 Metal−organic Frameworks. *New J. Chem.* **2016**, *40* (10), 8220−8224.
(25) DeCoste, J. B.; Weston, M. H.; Fuller, P. E.; Tovar, T. M.; Peterson, G. W.; LeVan, M. D.; Farha, O. K. Metal-Organic Frameworks for Oxygen Storage. *Angew. Chem., Int. Ed.* **2014**, *53* (51), 14092−14095.
(26) Min Wang, Q.; Shen, D.; Bülow, M.; Ling Lau, M.; Deng, S.; Fitch, F. R.; Lemcoff, N. O.; Semanscin, J. Metallo-Organic Molecular Sieve for Gas Separation and Purification. *Microporous Mesoporous Mater.* **2002**, *55* (2), 217−230.
(27) Sava Gallis, D. F.; Parkes, M. V.; Greathouse, J. A.; Zhang, X.; Nenoff, T. M. Enhanced O2 Selectivity versus N2 by Partial Metal Substitution in Cu-BTC. *Chem. Mater.* **2015**, *27* (6), 2018−2025.
(28) Weston, M. H.; Fuller, P.; Siu, P. W.-M. Metal-Organic Frameworks for Oxygen Storage and Air Separation, U.S. Patent US9427722B2, 2016.
(29) Sava Gallis, D. F.; Chapman, K. W.; Rodriguez, M. A.; Greathouse, J. A.; Parkes, M. V.; Nenoff, T. M. Selective O2 Sorption at Ambient Temperatures via Node Distortions in Sc-MIL-100. *Chem. Mater.* **2016**, *28* (10), 3327−3336.
(30) Yang, J.; Wang, Y.; Li, L.; Zhang, Z.; Li, J. Protection of Open-Metal V(III) Sites and Their Associated CO2/CH4/N2/O2/H2O Adsorption Properties in Mesoporous V-MOFs. *J. Colloid Interface Sci.* **2015**, *456*, 197−205.
(31) Bloch, E. D.; Murray, L. J.; Queen, W. L.; Chavan, S.; Maximoff, S. N.; Bigi, J. P.; Krishna, R.; Peterson, V. K.; Grandjean, F.; Long, G. J.; Smit, B.; Bordiga, S.; Brown, C. M.; Long, J. R. Selective Binding of O2 over N2 in a Redox−Active Metal−Organic Framework with Open Iron(II) Coordination Sites. *J. Am. Chem. Soc.* **2011**, *133* (37), 14814−14822.

DOI: 10.1021/acs.iecr.8b00981
Ind. Eng. Chem. Res. 2018, 57, 9240−9253

(32) Murray, L. J.; Dinca, M.; Yano, J.; Chavan, S.; Bordiga, S.; Brown, C. M.; Long, J. R. Highly-Selective and Reversible O2 Binding in Cr3(1,3,5-Benzenetricarboxylate)2. *J. Am. Chem. Soc.* **2010**, *132* (23), 7856−7857.
(33) Southon, P. D.; Price, D. J.; Nielsen, P. K.; McKenzie, C. J.; Kepert, C. J. Reversible and Selective O 2 Chemisorption in a Porous Metal−Organic Host Material. *J. Am. Chem. Soc.* **2011**, *133* (28), 10885−10891.
(34) Zhang, W.; Banerjee, D.; Liu, J.; Schaef, H. T.; Crum, J. V.; Fernandez, C. A.; Kukkadapu, R. K.; Nie, Z.; Nune, S. K.; Motkuri, R. K.; Chapman, K. W.; Engelhard, M. H.; Hayes, J. C.; Silvers, K. L.; Krishna, R.; McGrail, B. P.; Liu, J.; Thallapally, P. K. Redox-Active Metal-Organic Composites for Highly Selective Oxygen Separation Applications. *Adv. Mater.* **2016**, *28* (18), 3572−3577.
(35) Greathouse, J. A.; Teich-McGoldrick, S. L.; Allendorf, M. D. Molecular Simulation of Size-Selective Gas Adsorption in Idealised Carbon Nanotubes. *Mol. Simul.* **2015**, *41* (16−17), 1388−1395.
(36) Maximoff, S. N.; Smit, B. Redox Chemistry and Metal-Insulator Transitions Intertwined in a Nano-Porous Material. *Nat. Commun.* **2014**, *5*, 4032.
(37) Verma, P.; Maurice, R.; Truhlar, D. G. Identifying the Interactions That Allow Separation of O2 from N2 on the Open Iron Sites of Fe2(Dobdc). *J. Phys. Chem. C* **2015**, *119* (51), 28499−28511.
(38) Parkes, M. V.; Greathouse, J. A.; Hart, D. B.; Sava Gallis, D. F.; Nenoff, T. M. Ab Initio Molecular Dynamics Determination of Competitive O $_2$ vs. N $_2$ Adsorption at Open Metal Sites of M $_2$ (Dobdc). *Phys. Chem. Chem. Phys.* **2016**, *18* (16), 11528−11538.
(39) Moeljadi, A. M. P.; Schmid, R.; Hirao, H. Dioxygen Binding to Fe-MOF-74: Microscopic Insights from Periodic QM/MM Calculations. *Can. J. Chem.* **2016**, *94* (12), 1144−1150.
(40) Bloch, E. D.; Murray, L. J.; Queen, W. L.; Chavan, S.; Maximoff, S. N.; Bigi, J. P.; Krishna, R.; Peterson, V. K.; Grandjean, F.; Long, G. J.; Smit, B.; Bordiga, S.; Brown, C. M.; Long, J. R. Selective Binding of O2 over N2 in a Redox−Active Metal−Organic Framework with Open Iron(II) Coordination Sites. *J. Am. Chem. Soc.* **2011**, *133* (37), 14814−14822.
(41) Staniland, S. S.; Rawlings, A.; Bramble, J.; Tolosa, J.; Wilson, O.; García-Martínez, J. C.; Binns, C. *Adsorbents - Fundamentals and Applications*; Wiley: Weinheim, Germany, 2014; Vol. *6*.
(42) Gertler, J. *Out of Breath: Military Aircraft Oxygen Issues*; Congressional Research Service, 2017; Vol. *2017*.
(43) Yang, J.; Wang, Y.; Li, L.; Zhang, Z.; Li, J. Protection of open-metal V(III) sites and their associated $CO_2/CH_4/N_2/O_2/H_2O$ adsorption properties in mesoporous V-MOFs. *J. Colloid Interface Sci.* **2015**, *456*, 197−205.
(44) Vermoortele, F.; Bueken, B.; Le Bars, G.; Van de Voorde, B.; Vandichel, M.; Houthoofd, K.; Vimont, A.; Daturi, M.; Waroquier, M.; Van Speybroeck, V.; Kirschhock, C.; De Vos, D. E. Synthesis Modulation as a Tool To Increase the Catalytic Activity of Metal-Organic Frameworks: The Unique Case of UiO-66(Zr). *J. Am. Chem. Soc.* **2013**, *135* (31), 11465−11468.
(45) Shimomura, S.; Higuchi, M.; Matsuda, R.; Yoneda, K.; Hijikata, Y.; Kubota, Y.; Mita, Y.; Kim, J.; Takata, M.; Kitagawa, S. Selective Sorption of Oxygen and Nitric Oxide by an Electron-Donating Flexible Porous Coordination Polymer. *Nat. Chem.* **2010**, *2* (8), 633−637.
(46) Frenkel, D.; Smit, B. *Understanding Molecular Simulation: From Algorithms to Applications*, 2nd ed.; Academic Press, 2001.
(47) Wilmer, C. E.; Kim, K. C.; Snurr, R. Q. An Extended Charge Equilibration Method. *J. Phys. Chem. Lett.* **2012**, *3* (17), 2506−2511.
(48) Jiang, J. Molecular Simulations in Metal−organic Frameworks for Diverse Potential Applications. *Mol. Simul.* **2014**, *40* (7−9), 516−536.
(49) Keskin, S.; Liu, J.; Rankin, R. B.; Johnson, J. K.; Sholl, D. S. Progress, Opportunities, and Challenges for Applying Atomically Detailed Modeling to Molecular Adsorption and Transport in Metal - Organic Framework Materials. *Ind. Eng. Chem. Res.* **2009**, *48* (5), 2355−2371.
(50) Düren, T.; Bae, Y.-S.; Snurr, R. Q. Using Molecular Simulation to Characterise Metal−organic Frameworks for Adsorption Applications. *Chem. Soc. Rev.* **2009**, *38* (5), 1237.
(51) Yang, Q.; Liu, D.; Zhong, C.; Li, J. Development of Computational Methodologies for Metal − Organic Frameworks and Their Application in Gas Separations. *Chem. Rev.* **2013**, *113* (10), 8261−8323.
(52) Fischer, M.; Gomes, J. R. B.; Jorge, M. Computational approaches to study adsorption in MOFs with unsaturated metal sites. *Mol. Simul.* **2014**, *40*, 537−556.
(53) Chen, L.; Grajciar, L.; Nachtigall, P.; Düren, T. Accurate Prediction of Methane Adsorption in a Metal-Organic Framework with Unsaturated Metal Sites by Direct Implementation of an Ab Initio Derived Potential Energy Surface in GCMC Simulation. *J. Phys. Chem. C* **2011**, *115* (46), 23074−23080.
(54) Getzschmann, J.; Senkovska, I.; Wallacher, D.; Tovar, M.; Fairen-Jimenez, D.; Düren, T.; van Baten, J. M.; Krishna, R.; Kaskel, S. Methane Storage Mechanism in the Metal-Organic Framework Cu3(Btc)2: An in Situ Neutron Diffraction Study. *Microporous Mesoporous Mater.* **2010**, *136* (1−3), 50−58.
(55) Zeitler, T. R.; Van Heest, T.; Sholl, D. S.; Allendorf, M. D.; Greathouse, J. A. Predicting Low-Pressure O2 Adsorption in Nanoporous Framework Materials for Sensing Applications. *ChemPhysChem* **2013**, *14* (16), 3740−3750.
(56) Koh, K.; Wong-Foy, A. G.; Matzger, A. J. A Crystalline Mesoporous Coordination Copolymer with High Microporosity. *Angew. Chem., Int. Ed.* **2008**, *47* (4), 677−680.
(57) Dubbeldam, D.; Calero, S.; Ellis, D. E.; Snurr, R. Q. *RASPA 1.0: Molecular Software Package for Adsorption and Diffusion in Flexible Nanoporous Materials*, 2013.
(58) Dubbeldam, D.; Calero, S.; Ellis, D. E.; Snurr, R. Q. RASPA: Molecular Simulation Software for Adsorption and Diffusion in Flexible Nanoporous Materials. *Mol. Simul.* **2016**, *42* (2), 81−101.
(59) Eddaoudi, M.; Kim, J.; Rosi, N.; Vodak, D.; Wachter, J.; O'Keeffe, M.; Yaghi, O. M. Systematic Design of Pore Size and Functionality in Isoreticular MOFs and Their Application in Methane Storage. *Science* **2002**, *295* (5554), 469−472.
(60) Cavka, J. H.; Jakobsen, S.; Olsbye, U.; Guillou, N.; Lamberti, C.; Bordiga, S.; Lillerud, K. P. A New Zirconium Inorganic Building Brick Forming Metal Organic Frameworks with Exceptional Stability. *J. Am. Chem. Soc.* **2008**, *130* (42), 13850−13851.
(61) Chui, S. S. Y.; Lo, S. M. F.; Charmant, J. P. H.; Orpen, a G.; Williams, I. D. A Chemically Functionalizable Nanoporous Material [Cu3(TMA)2(H2O)3]n. *Science* **1999**, *283*, 1148−1150.
(62) Rappe, A. K.; Casewit, C. J.; Colwell, K. S.; Goddard, W. A., III; Skiff, W. M. UFF, a full periodic table force field for molecular mechanics and molecular dynamics simulations. *J. Am. Chem. Soc.* **1992**, *114* (25), 10024−10035.
(63) Mayo, S. L.; Olafson, B. D.; Goddard, W. A. DREIDING: A Generic Force Field for Molecular Simulations. *J. Phys. Chem.* **1990**, *94* (26), 8897−8909.
(64) Eggimann, B. L.; Sunnarborg, A. J.; Stern, H. D.; Bliss, A. P.; Siepmann, J. I. An Online Parameter and Property Database for the TraPPE Force Field. *Mol. Simul.* **2014**, *40* (1−3), 101−105.
(65) Vuong, T.; Monson, P. A. Monte Carlo Simulation Studies of Heats of Adsorption in Heterogeneous Solids. *Langmuir* **1996**, *12* (22), 5425−5432.
(66) Talu, O.; Myers, A. L. Molecular Simulation of Adsorption: Gibbs Dividing Surface and Comparison with Experiment. *AIChE J.* **2001**, *47* (5), 1160−1168.
(67) Düren, T.; Millange, F.; Férey, G.; Walton, K. S.; Snurr, R. Q. Calculating Geometric Surface Areas as a Characterization Tool for Metal - Organic Frameworks. *J. Phys. Chem. C* **2007**, *111* (42), 15350−15356.
(68) Gelb, L. D.; Gubbins, K. E. Pore Size Distributions in Porous Glasses: A Computer Simulation Study. *Langmuir* **1999**, *15* (2), 305−308.

DOI: 10.1021/acs.iecr.8b00981
Ind. Eng. Chem. Res. 2018, 57, 9240−9253

(69) Walton, K. S.; Sholl, D. S. Predicting Multicomponent Adsorption: 50 Years of the Ideal Adsorbed Solution Theory. *AIChE J.* **2015**, *61* (9), 2757−2762.
(70) Chen, H.; Sholl, D. S. Examining the Accuracy of Ideal Adsorbed Solution Theory without Curve-Fitting Using Transition Matrix Monte Carlo Simulations. *Langmuir* **2007**, *23* (11), 6431−6437.

DOI: 10.1021/acs.iecr.8b00981
Ind. Eng. Chem. Res. 2018, 57, 9240−9253